

Propagation properties of the chirped Airy-Gaussian vortex electron plasma wave

Lican Wu(吴利灿), Jinhong Wu(吴锦鸿), Yujun Liu(刘煜俊), and Dongmei Deng(邓冬梅)†

Citation: Chin. Phys. B, 2020, 29 (**12**): 125202. DOI: 10.1088/1674-1056/aba9cc
Journal homepage: http://cpb.iphy.ac.cn; http://iopscience.iop.org/cpb

What follows is a list of articles you may be interested in

Analysis of Landau damping in radially inhomogeneous plasma column

H Rajabalinia-Jelodar, M K Salem, F M Aghamir, H Zakeri-Khatir
Chin. Phys. B, 2018, 27 (**5**): 055203. DOI: 10.1088/1674-1056/27/5/055203

Pulse chirping effect on controlling the transverse cavity oscillations in nonlinear bubble regime

H Vosoughian, Z Riazi, H Afarideh, G Sarri
Chin. Phys. B, 2017, 26 (**2**): 025201. DOI: 10.1088/1674-1056/26/2/025201

Landau damping in a bounded magnetized plasma column

H. Zakeri-Khatir, F. M. Aghamir
Chin. Phys. B, 2015, 24 (**2**): 025201. DOI: 10.1088/1674-1056/24/2/025201

Electromagnetic interaction between local surface plasmon polaritons and an atmospheric surface wave plasma jet

Chen Zhao-Quan, Hu Dong, Liu Ming-Hai, Xia Guang-Qing, Zheng Xiao-Liang, Hu Ye-Lin, Ye Qiu-Bo, Chen Ming-Gong, Zhu Long-Ji, Hu Xi-Wei
Chin. Phys. B, 2014, 23 (**3**): 035202. DOI: 10.1088/1674-1056/23/3/035202

Monoenergetic electron parameters in a spheroid bubble model

H. Sattarian, Sh. Rahmatallahpur, T. Tohidi
Chin. Phys. B, 2013, 22 (**2**): 025203. DOI: 10.1088/1674-1056/22/2/025203

Propagation properties of the chirped Airy–Gaussian vortex electron plasma wave*

Lican Wu(吴利灿), Jinhong Wu(吴锦鸿), Yujun Liu(刘煜俊), and Dongmei Deng(邓冬梅)†

Guangdong Provincial Key Laboratory of Nanophotonic Functional Materials and Devices, South China Normal University, Guangzhou 510631, *China*

(Received 19 May 2020; revised manuscript received 15 July 2020; accepted manuscript online 28 July 2020)

We introduce a new class of the chirped Airy–Gaussian vortex electron plasma (CAiGVEP) wave which constitutes the exact and continuous transition modes between the chirped Airy vortex and the chirped Gaussian vortex electron plasma wave. The intensity, the phase, and the angular momentum density flow of the CAiGVEP wave are discussed under different distribution factors and different chirp modes.

Keywords: Airy–Gaussian wave, plasma wave, chirp

PACS: 52.35.Hr, 52.35.Mw **DOI:** 10.1088/1674-1056/aba9cc

1. Introduction

In recent years, the interaction between laser and plasma had attracted the attention of many people. Then, Stix investigated waves in the plasma in 1992.[1] Salandrino and Christodoulides introduced a new class of nondiffracting surface plasmonic waves, the Airy plasmon.[2] Then in recent years, Naveen and Arvinder mainly discussed the effect of cross-focusing of two q-Gaussian laser beams on the excitation of electron plasma waves in an underdense plasma with collisional nonlinearity which was detective.[3] Ouahid *et al.* studied the relativistic self-focusing of finite Airy–Gaussian beams in collisionless plasma using the Wentzel–Kramers–Brillouin approximation.[4] Just this year, effects of dust-charge gradient and polarization forces on the waves and Jeans instability in strongly coupled dusty plasma were also explored.[5]

As for Airy beams or Airy–Gaussian beams, with the support of quantum mechanics, Berry and Balazs foresaw that the basic Airy wave packet would be a solution of the Schrödinger equation in 1979.[6] Because of several unique properties of Airy beams, namely, non-diffracting,[7] self-acceleration,[8] self-focusing,[9] and self-healing,[10] so many researchers had done a lot of researches. At present, Airy beams had also made many advances in applications, such as optical cleaning of particles,[11] light bullets,[12] and microscopy.[13] Recently, Xu *et al.* studied the radially polarized symmetric Airy beam and found some interesting properties.[14] The Airy–Gaussian (AiG) beams propagate with a period between Airy beams and Gaussian beams, which is controlled by a factor. And the AiG beams were well verified experimentally.[15]

The chirp factor is a variable that changes over time. In the early 1990s, Melinger *et al.* conducted their first experiment using simple linear chirped laser pulses.[16] The chirped Bessel waves were studied in 2015 and the researchers got their properties.[17] Shi *et al.* numerically analyzed dynamic propagation of symmetric Airy pulses with initial chirps in an optical fiber.[18] Then, in 2018, Xie *et al.* gave their findings about the first-order chirped Airy vortex beams in a chiral medium.[19] Further, the chirped Airy–Gaussian vortex beams in chiral medium were discussed by Zhou *et al* in the same year.[19] Both Yang and Chen had done researches on the transmission characteristics of chirped Airy–Gaussian beams in a harmonic potential in 2019.[21,22]

Therefore, in this paper, we propose the chirped Airy–Gaussian vortex electron plasma (CAiGVEP) wave by multiplying Airy function, Gaussian function, vortex factor, and chirp factor. And we mainly discuss the properties of CAiGVEP wave of $M = 1$ (*i.e*, the first-order vortex).

2. Equation of chirped Airy–Gaussian vortex electron plasma wave

Generally speaking, based on existing theory, we can write the wave function as following form:

$$\tilde{n}(r,z,t) = \tilde{n}_0(r,z)\exp(\mathrm{i}kz - \mathrm{i}wt), \tag{1}$$

which is a function of time and space. In this function, $\tilde{n}$ is the perturbed electron density with equilibrium value n_0, $\tilde{n}_0(r,z)$ is the CAiGVEP wave function in form of cylindrical coordinates and $r = \sqrt{x^2+y^2}$. The longitudinal wave number k is set to satisfy linear dispersion relation $k^2 S_\mathrm{e} = \omega^2 - \omega_\mathrm{pe}^2$. $S_\mathrm{e} = (3k_\mathrm{b}T_\mathrm{e}/m_\mathrm{e})^{1/2}$ is electron thermal speed, T_e is electron temperature, k_b is the Boltzmann constant, m_e is electron mass, and

*Project supported by the National Natural Science Foundation of China (Grant Nos. 11775083 and 11374108), the Science and Technology Program of Guangzhou City (Grant No. 2019050001), and the Special Funds for the Cultivation of Guangdong College Students' Scientific and Technological Innovation (Grant Nos. pdjh2020a0149 and pdjh2019a0127).

†Corresponding author. E-mail: dmdeng@263.net

© 2020 Chinese Physical Society and IOP Publishing Ltd

$\omega_{\rm pe} = (4\pi e^2 n_0/m_{\rm e})^{1/2}$ is electron plasma frequency. Then, in order to obtain the satisfied equation of electron plasma wave, we give the plasma model containing unmagnetized collision-free neutral particles and inertial electrons. Therefore, the corresponding equation is

$$\left(\frac{\partial^2}{\partial t^2}\right) - S_{\rm e}^2\nabla^2 + \omega_{\rm pe}^2)\tilde{n} = 0. \tag{2}$$

By substituting Eq. (1) into Eq. (2) we obtain the simplified equation

$$\left(\nabla_\perp^2 + 2{\rm i}k\frac{\partial}{\partial z}\right)\tilde{n}_{\ 0}(r,z) = 0. \tag{3}$$

In modern optical theory, we can express the CAiGVEP wave in the initial plane as

$$\begin{aligned}\tilde{n}_0(r,0) \ =\ & \tilde{N}_0{\rm Ai}\left(\frac{x}{w_0}\right){\rm Ai}\left(\frac{y}{w_0}\right)\\ & \times\exp\left(a\frac{x}{w_0}+b\frac{y}{w_0}-\left(\chi_0\frac{x}{w_0}\right)^2-\left(\chi_0\frac{y}{w_0}\right)^2\right)\\ & \times\exp\left(-{\rm i}\left(\beta_{1x}\frac{x}{w_0}+\beta_{1y}\frac{y}{w_0}+\beta_{2x}\left(\frac{x}{w_0}\right)^2\right.\right.\\ & \left.\left.+\beta_{2y}\left(\frac{y}{w_0}\right)^2\right)\right)\left(\frac{x}{w_0}+{\rm i}\frac{y}{w_0}\right)^M,\end{aligned} \tag{4}$$

where $\tilde{N}_0$ is the maximum amplitude of the CAiGVEP wave, a and b are decay factors ranging from 0 to 1, χ is distribution factor which tends toward Airy vortex beams with a smaller value or Gaussian vortex beams with a larger one, β_{1x} and β_{1y} indicate the first-order chirp parameters, β_{2x} and β_{2y} indicate the second-order chirp parameters, M is topological charge, w_0 is an arbitrary transverse scale. In order to obtain the analytical solution of the wave, we used the following Airy integral formula:

$$\begin{aligned}&\int{\rm Ai}\left(\frac{x}{a}\right)\exp\left(bx^2+cx\right){\rm d}x\\ =\ &\sqrt{\frac{-\pi}{b}}\exp\left(-\frac{c^2}{4b}+\frac{c}{8a^3b^2}-\frac{1}{96a^6b^3}\right)\\ &\times{\rm Ai}\left(\frac{1}{16a^4b^2}-\frac{c}{2ab}\right).\end{aligned} \tag{5}$$

By substituting Eq. (4) into Eq. (3), we get the exact analytical equation after using the integral formula and the Fourier transform

$$\begin{aligned}\tilde{n}_0(r,z) \ =\ & -\sum_{m=0}^{M}{\rm i}^M C_M^m\frac{\partial^{M-m}}{\partial a^{M-m}}\frac{\partial^m}{\partial b^m}\tilde{N}_0\\ & \times\sqrt{\frac{b_1b_1^*}{b_2b_2^*}}{\rm Ai}\left[\frac{1}{16b_2^2}-\frac{c_2}{2b_2}\right]\\ & \times\exp\left(-\frac{c_2^2}{4b_2}+\frac{c_2}{8b_2^2}-\frac{1}{96b_2^3}\right)\\ & \times\exp\left[\frac{{\rm i}z}{4Zr}\left(\frac{1}{64b_1^2}-\frac{a_1}{4b_1}+a_1^2\right)\right.\\ & \left.-\frac{x}{w_0}\left(\frac{1}{8b_1}-a_1\right)+\frac{1}{768b_1^3}\right]\\ & \times{\rm Ai}\left[\frac{1}{16b_2^{*2}}-\frac{c_2^*}{2b_2^*}\right]\\ & \times\exp\left(-\frac{c_2^{*2}}{4b_2^*}+\frac{c_2^*}{8b_2^{*2}}-\frac{1}{96b_2^{*3}}\right)\\ & \times\exp\left[\frac{{\rm i}z}{4Zr}\left(\frac{1}{64b_1^{*2}}-\frac{a_1^*}{4b_1^*}+a_1^{*2}\right)\right.\\ & \left.-\frac{y}{w_0}\left(\frac{1}{8b_1^*}-a_1^*\right)+\frac{1}{768b_1^{*3}}\right],\end{aligned} \tag{6}$$

where

$$\begin{aligned}&a_1 = a-{\rm i}\beta_{1x},\quad b_1 = {\rm i}\beta_{2x}-\chi_0,\quad b_2 = -b_1+{\rm i}b_1^2\frac{z}{Zr},\\ &c_2 = -\frac{1}{8b_1}-{\rm i}\frac{z}{8Zr}+{\rm i}a_1b_1\frac{z}{Zr}+2b_1\frac{x}{w_0},\\ &a_1^* = b^*-{\rm i}\beta_{1y},\quad b_1^* = {\rm i}\beta_{2y}-\chi_0,\quad b_2^* = -b_1^*+{\rm i}b_1^{*2}\frac{z}{Zr},\\ &c_2^* = -\frac{1}{8b_1^*}-{\rm i}\frac{z}{8Zr}+{\rm i}a_1^*b_1^*\frac{z}{Zr}+2b_1^*\frac{y}{w_0},\\ &Zr = kw_0^2,\end{aligned} \tag{7}$$

and Zr is Rayleigh range.

3. Discussion and annlysis

So, we set some parameters like the unperturbed electron density of plasma when the electron density distribution of finite-energy chirped Airy–Gaussian vortex plasma mode is discussed in the x–y plane $n_{\rm eo} = 10^{15}$ cm^{-3}, electron temperature $T_{\rm e} = 10^6$ K, electron density perturbation $\tilde{N}_0 \sim 0.1n_{\rm e0}$, arbitrary transverse scale $w_0 = 5\lambda$, and attenuation factors $a = b = 0.05$. The first-order chirp factor is set as $\beta_1 = \beta_{1x} = \beta_{2y}$ and the second-order chirp factor is set as $\beta_2 = \beta_{2x} = \beta_{2y}$. So, when $\beta_1 \neq 0$ and $\beta_2 = 0$, the first-order chirped Airy–Gaussian vortex electron plasma wave can be obtained. It follows the same way to get the second-order chirped Airy–Gaussian vortex electron plasma wave by setting $\beta_1 = 0$ and $\beta_2 \neq 0$. In order to better study this wave, we also discuss these cases with different distribution factors.

When the wave just emits, the intensity mainly distributes in side lobes as shown in Fig. 1. With the distance increasing, the energy concentrates towards main lobe and the area of intensity distribution becomes smaller. However, when it comes to $z = 6Zr$, the energy of main lobe spreads to lower left, which results in a fan-shaped distribution at $z = 16Zr$. We can see that propagation features are roughly the same when the chirp β_1 increases, but the difference is that the larger the chirp factor is, the smaller the distribution area at the same distance is. In addition, the distribution is closer to lower left corner with larger chirp factor.

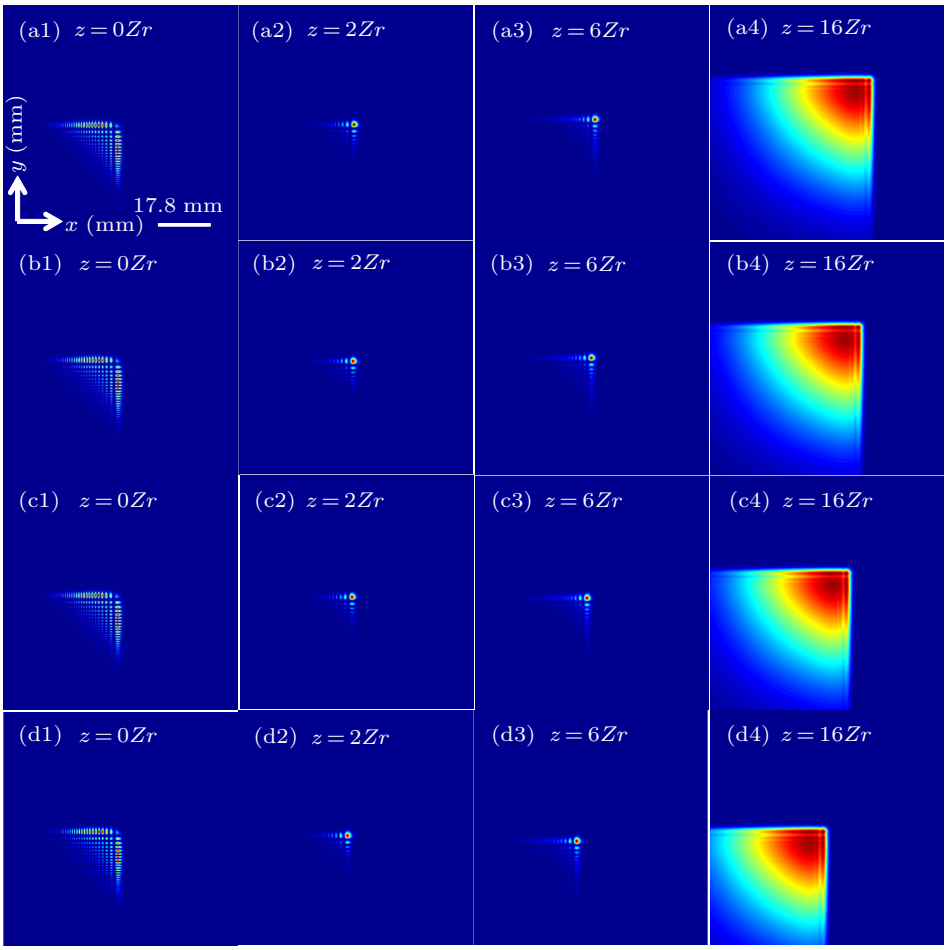


Fig. 1. The cross-sectional intensity of the CAiGVEP wave during propagation at different chirp factors when $\chi_0 = 0.05$, $\beta_1 \neq 0$, and $\beta_2 = 0$. Panels (a1)–(a4), (b1)–(b4), (c1)–(c4), and (d1)–(d4) are distributions when $\beta_1 = 0.05$, $\beta_1 = 0.5$, $\beta_1 = 1$, $\beta_1 = 2$, respectively.

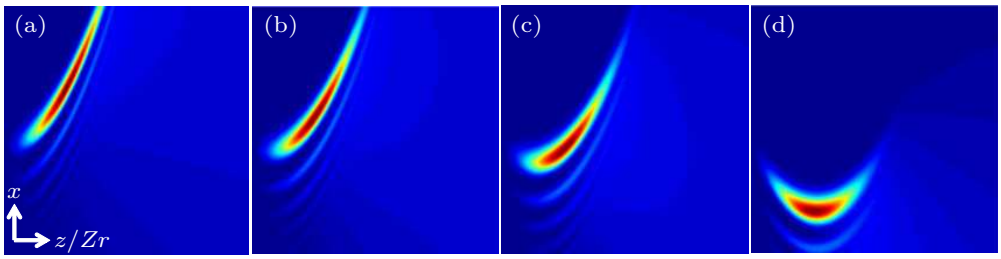


Fig. 2. The intensity distribution with different chirp factors of the CAiGVEP wave on the x–z plane when $\chi_0 = 0.05$, $\beta_1 \neq 0$, and $\beta_2 = 0$. Panels (a)–(d) are distributions when $\beta_1 = 0.05$, $\beta_1 = 0.5$, $\beta_1 = 1$, $\beta_1 = 2$, respectively.

In the case of single chirp factor in Fig. 2, this wave focuses on the top in the x–z plane and below it has some faint distributions. The first-order CAiGVEP wave is approximately parabolic, and the intensity distributions are narrow and long when the chirp factor is small. As the chirp factor β_1 increases, the curvature of these distributions becomes smaller and the wave is positioned closer to the z axis.

Although the intensity distributions show similarities, the phase distributions in Fig. 3 are quite different. When $\beta_1 = 0.05$, we can see from Fig. 3(a1) that the phase distribution is even in the first quadrant. When the propagation gets further, the phase distribution is spiral and gets more regular. As it comes to Fig. 3(a4), a more complete vortex-like phase distribution brings uniformity. However, as the chirp parameter β_1 gets larger to 0.5, the initial phase distribution in Fig. 3(b1) shows like Fig. 3(a2). And at $z = 2Zr$ the distribution of the first quadrant is very uniform in Fig. 3(b2). As the chirp factor increases to 1 or 2, it is different that the vortex-like phase distribution also begins to appear in the initial plane such as Figs. 3(c1) and 3(d1). The formation of vortex distribution at $z = 16Zr$ is their common feature.

The electrostatic potential $V(x,y,z,t)$ is closely related to electron density disturbance. The relationship between them can be written in the following form:[23]

$$\nabla^2 V = 4\pi e\tilde{n}. \tag{8}$$

Considering paraxial approximation, we can give the formula of electrostatic potential in form of a wave function

$$V(x,y,z,t) = \tilde{V}(x,y,z)\exp(\mathrm{i}kz - \mathrm{i}wt), \tag{9}$$

putting Eq. (9) into Eq. (8), the following equation can be obtained:

$$\left(\nabla_{\perp}^2 + 2\mathrm{i}k\frac{\partial}{\partial z}\right)\tilde{V} - k^2\tilde{V} = 4\pi e\tilde{n}_0. \tag{10}$$

Following the previous method, we get

$$k^2\tilde{V} = -4\pi e\tilde{n}_0, \tag{11}$$

so electrostatic potential caused by this wave can be expressed as

$$V(x,y,z) = -\frac{4\pi e}{k^2}\tilde{n}_0. \tag{12}$$

According to the relationship between electrostatic potential and electric field, the electric field can be expressed by electrostatic potential

$$\boldsymbol{E}(x,y,z) = -\mathrm{i}\boldsymbol{k}_{\mathrm{ef}}V, \tag{13}$$

where $\boldsymbol{k}_{\mathrm{ef}}$ is composed of effective wave vectors of waves on each component

$$\boldsymbol{k}_{\mathrm{ef}} = \left(\frac{\mathrm{i}\partial\tilde{n}}{\tilde{n}\partial x}, \frac{\mathrm{i}\partial\tilde{n}}{\tilde{n}\partial y}, \frac{\mathrm{i}\partial\tilde{n}}{\tilde{n}\partial z} - \mathrm{i}k\right). \tag{14}$$

In plasma physics, the energy flow has a predetermined relationship with group velocity

$$\boldsymbol{T} = W\boldsymbol{v}_{\mathrm{g}}, \tag{15}$$

where the electron group velocity $\boldsymbol{v}_{\mathrm{g}} = v_{\mathrm{g}}\boldsymbol{e}_{\mathrm{ef}}$, the unit wave vector parallel to electric field $\boldsymbol{e}_{\mathrm{ef}} = \boldsymbol{k}_{\mathrm{ef}}/k_{\mathrm{ef}}$, W is electron density associated with the CAiGVEP wave,[23]

$$W = \frac{|E|^2 A(k,\omega)}{16\pi},$$
$$A(k,\omega) = 1 + \omega_{\mathrm{pe}}^2\frac{(\omega^2 + k^2S_{\mathrm{e}}^2)}{(\omega^2 - k^2S_{\mathrm{e}}^2)^2}. \tag{16}$$

Therefore, the time-averaged angular momentum density flow can be obtained based on angular momentum density, as follows:

$$\boldsymbol{M} = \frac{1}{4\pi}(\boldsymbol{r}\times\boldsymbol{T}). \tag{17}$$

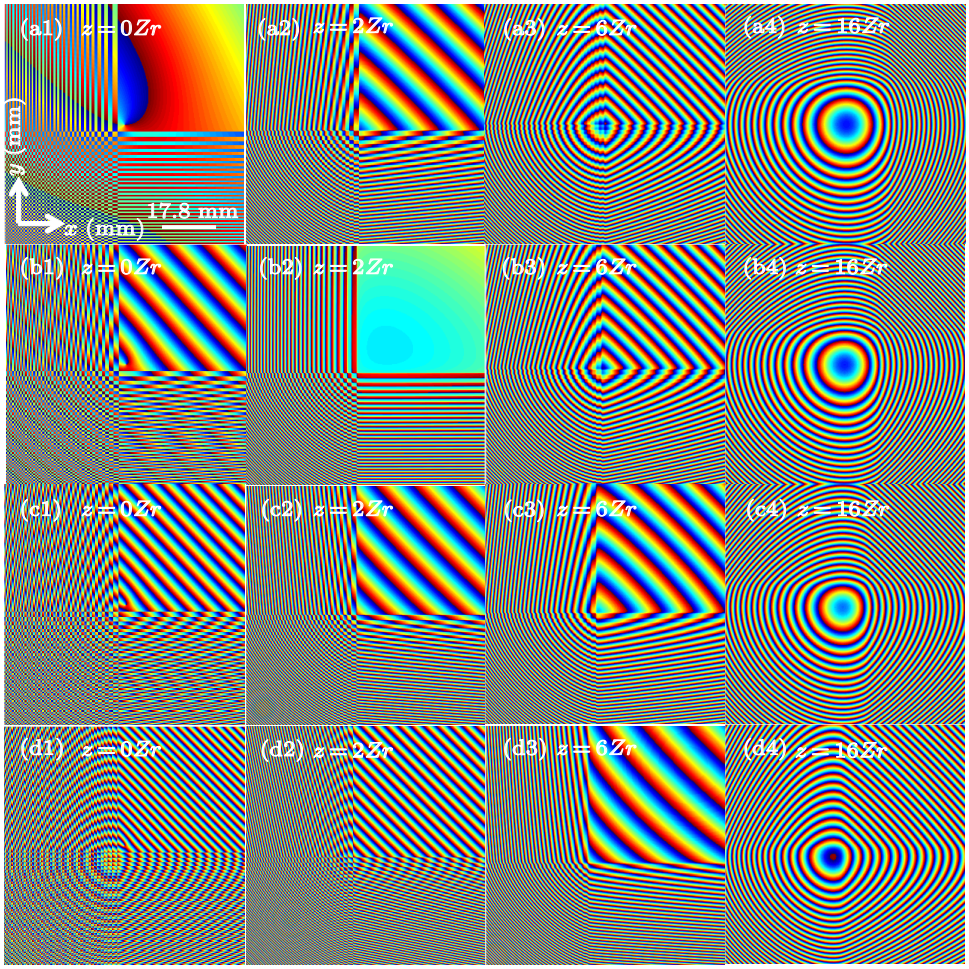


Fig. 3. Phase distribution ($x = y$) of the CAiGVEP wave during propagation at different chirp factors when $\chi_0 = 0.05$, $\beta_1 \neq 0$, and $\beta_2 = 0$. Panels (a1)–(a4), (b1)-(b4), (c1)—(c4), and (d1)–(d4) are distributions when $\beta_1 = 0.05$, $\beta_1 = 0.5$, $\beta_1 = 1$, $\beta_1 = 2$, respectively.

The angular momentum density flow symmetrically distributes about the $y = x$ direction in Fig. 4 when the chirp factor β_1 is 0.05. When the wave is just formed, the angular momentum density flow distributes in the y and x directions. And then the flow of main lobe appears in the $y = x$ direction. Then, the directions of flow change to the $y = x$ direction and the entire angular momentum density flow profile is tapered when the wave goes further. Increasing the chirp factor β_1 to 1 or 2, the flow shares some common characteristics with the flow of $\beta_1 = 0.05$ and 0.5. The obvious difference is that the angular momentum density flow distribution gradually shrinks, and the cone distribution becomes less conical.

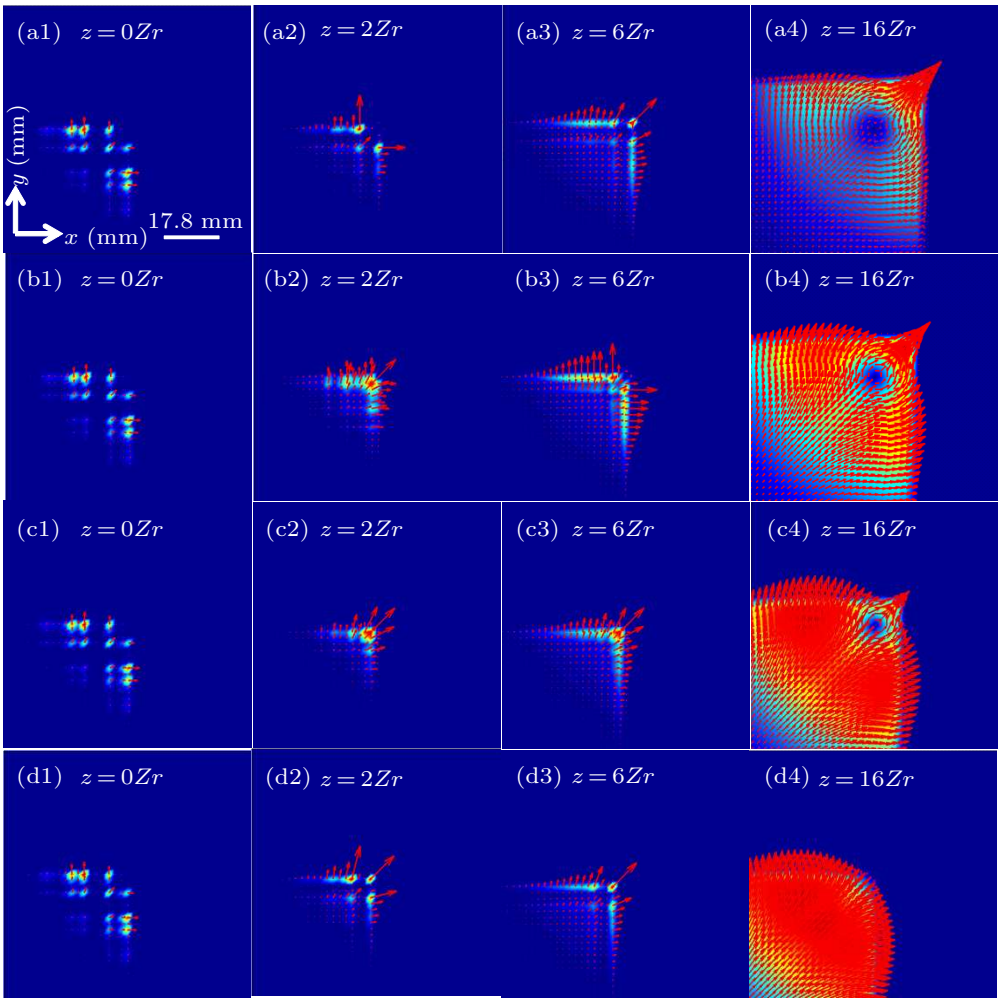


Fig. 4. Angular momentum density flow ($x = y$) of the CAiGVEP wave during propagation at different chirp factors when $\chi_0 = 0.05$, $\beta_1 \neq 0$, and $\beta_2 = 0$. Panels (a1)–(a4), (b1)–(b4), (c1)–(c4), and (d1)–(d4) are distributions when $\beta_1 = 0.05$, $\beta_1 = 0.5$, $\beta_1 = 1$, $\beta_1 = 2$, respectively.

For intensity in Fig. 5, the second-order CAiGVEP wave behaves similar to the first-order CAiGVEP wave when $\beta_1 = 0.05$. For instance, the intensity focuses on side lobes and then goes to main lobe, which is accompanied by a significant reduction in the focus range. At $z = 12Zr$, the entire distribution appears as a triangular distribution due to the diffusion of energy. There is a quite different thing that the energy does not spread back when the chirp factor β_2 grows larger. When β_2 becomes 0.5, we find that intensity distribution will reverse and focus on the side lobes like the initial field by comparing Fig. 5(b4) to Fig. 5(b3). Before reversing, energy still converges towards main lobe. Apparently, the inversion distance is approximately $z = 2Zr$ when $\beta_2 = 0.5$. After the inversion, the energy stays in side lobes without converging to main lobe. At the same time, the focusing range of side lobes is getting wider. The reversal point gets closer and closer to the starting point when the chirp β_2 increases. We can estimate that when $\beta_2 = 1$, the reversal point is at $z = 1Zr$, and when $\beta_2 = 2$, it is at $z = 0.5Zr$.

We can see the intensity distribution on the x–z plane in the Fig. 6. When the second chirp factor is 0.05, the intensity distribution is parabolic, like the distribution of the same chirp factor. But, it is very different when the chirp factor increases to 0.5, 1, and 2. There are obvious discontinuities in the intensity distribution. The position of these discontinuities happens to be at the point of reversal. And at the same time, the intensity distribution is not so concentrated.

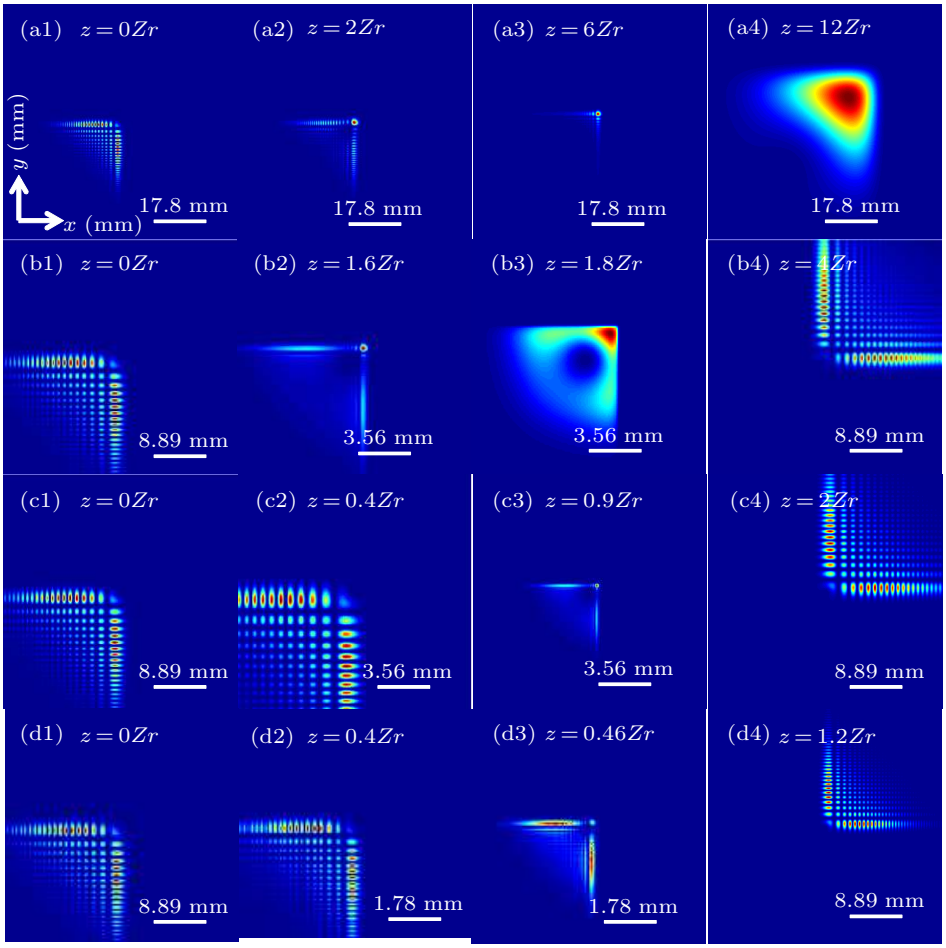


Fig. 5. The cross-sectional intensity of the CAiGVEP wave during propagation at different chirp factors when $\chi_0 = 0.05$, $\beta_1 = 0$, and $\beta_2 \neq 0$. Panels (a1)–(a4), (b1)–(b4), (c1)–(c4), and (d1)–(d4) are distributions when $\beta_2 = 0.05$, $\beta_2 = 0.5$, $\beta_2 = 1$, $\beta_2 = 2$, respectively.

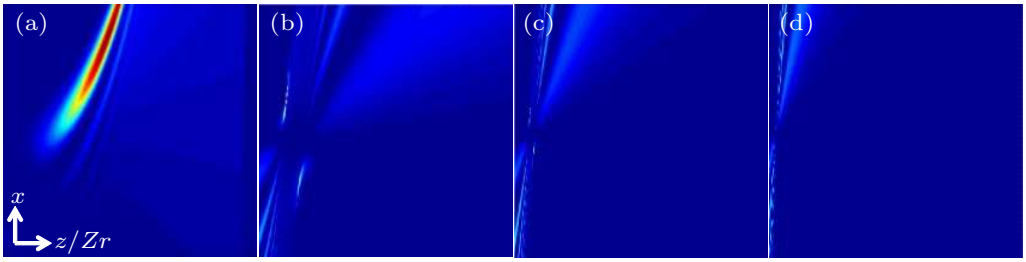


Fig. 6. The intensity distribution on the x–z plane with different chirp factors for the CAiGVEP wave when $\chi_0 = 0.05$, $\beta_1 = 0$, and $\beta_2 \neq 0$. Panels (a)–(d) are distributions when $\beta_2 = 0.05$, $\beta_2 = 0.5$, $\beta_2 = 1$, $\beta_2 = 2$, respectively.

The angular momentum density flow of side lobes in Fig. 7 is along the x and y directions, while the direction of angular momentum density flow of main lobe is along the $y = x$ direction. Similarly, the angular momentum density flow has a conical distribution due to the change in the direction of angular momentum density flow of side lobes. In the two side lobes, the angular momentum density flow distribution along the x-axis direction is more pronounced and stronger with the chirp factor becoming 0.5. However, as the wave propagates farther and reverses, the angular momentum density flow distribution also reverses. At this time, the stronger performance is replaced by the angular momentum density flow flowing along the y axis, such as Figs. 6(b4), 6(c4), and 6(d4). However, the unilateral enhancement effect weakens as β_2 increases, which is easy to be found by comparing the processes of $\beta_2 = 0.5$, 1, and 2.

We calculate the case where distribution factor is $\chi_0 = 1$ for comparison. In Fig. 8, an uneven circular distribution appears on the initial plane and its distribution range is small. By increasing propagation distances, the focusing part slowly turns clockwise from bottom left and at the same time the intensity range becomes larger. As you can see, the ring-like intensity distribution is very obvious in this case. We also increase the first-order chirp factor, and find that there is basically no change, except that the distribution location changes slightly at the same distance.

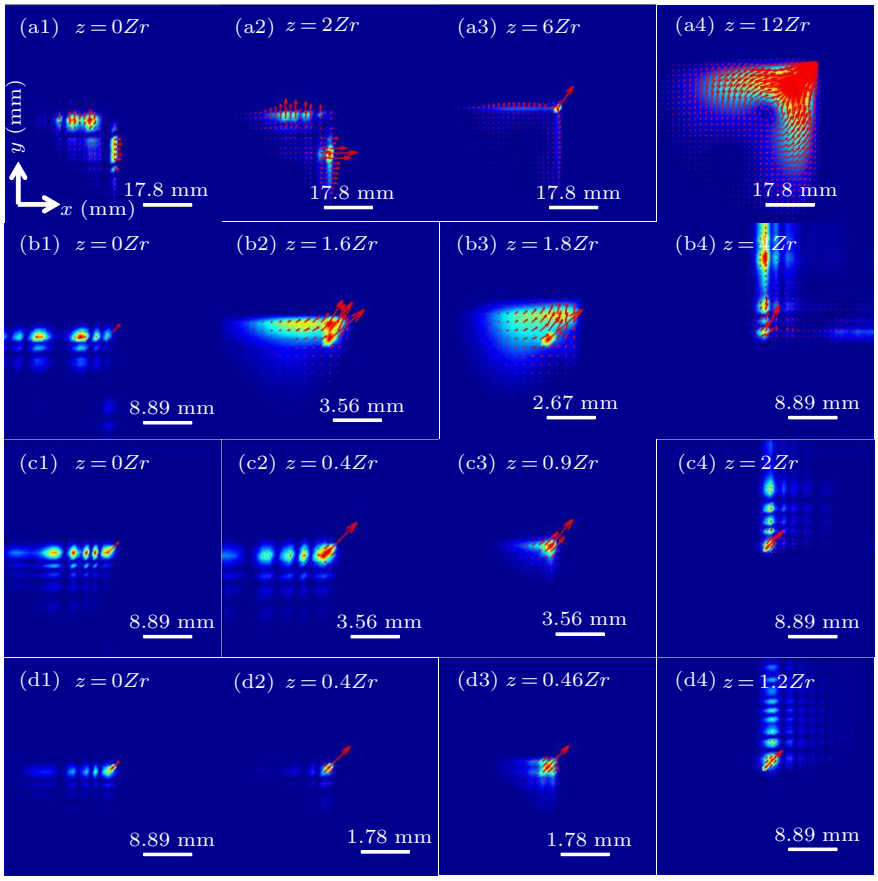


Fig. 7. Angular momentum density flow ($x=y$) of the CAiGVEP wave during propagation at different chirp factors when $\chi_0=0.05$, $\beta_1=0$, and $\beta_2\neq 0$. Panels (a1)–(a4), (b1)–(b4), (c1)–(c4), and (d1)–(d4) are distributions when $\beta_2=0.05$, $\beta_2=0.5$, $\beta_2=1$, $\beta_2=2$, respectively.

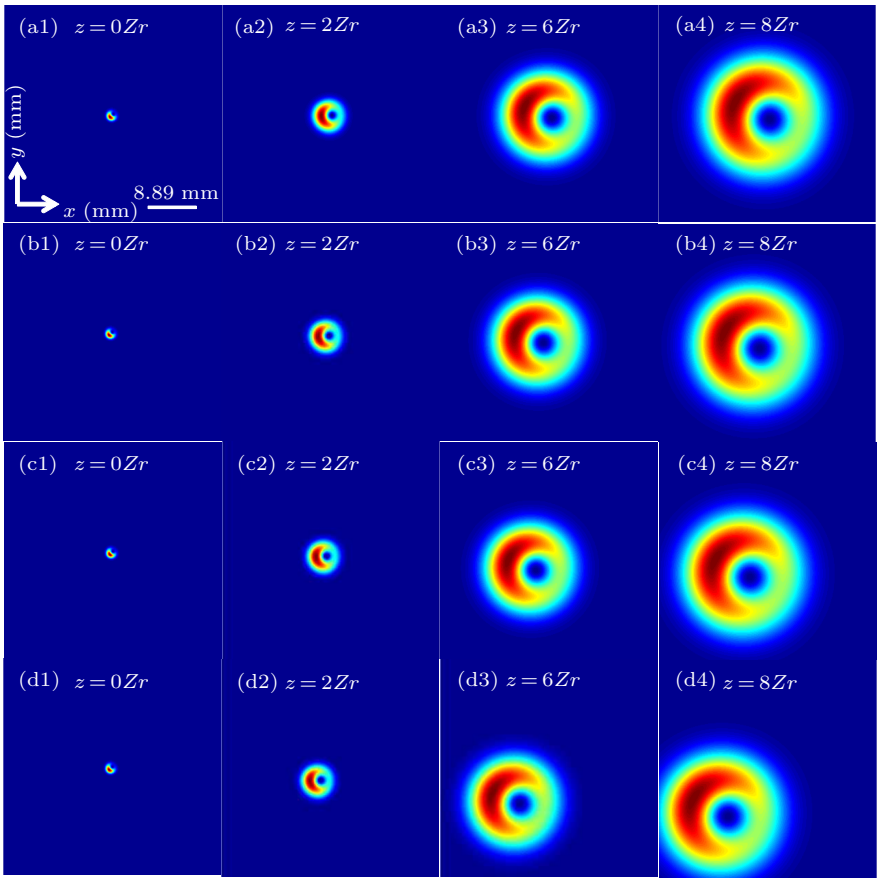


Fig. 8. All are the same as those in Fig. 1 except $\chi_0=1$.

Similarly, we can see from Fig. 9 that the intensity distribution changes in the x–z plane. The entire distribution presents a parabolic shape with an opening down on the plane. When the chirping factor is relatively high, it presents a more narrower and longer distribution, and is closer to the x axis. And the focusing range is larger.

To match this case, we complete angular momentum density flow analysis. The size of angular momentum density flow distribution is proportional to intensity distribution in Fig. 10. When $\beta_1 = 0.05$, the left half gathers most of angular momentum density flow distribution. However, the directions of angular momentum density flow in left half and right half tend to converge toward the $y = x$ direction. When β_1 comes to 0.5, 1, and 2, the three cases have a very high degree of similarity but are almost different from the case of $\beta_1 = 0.05$. The angular momentum density flow is basically concentrated in left half, and the direction uniformly points to upper right. Obviously, the slope of the direction increases as β_1 increases, getting closer to the y axis.

We added Fig. 11 as a supplement to the effect on β_2. We also saw an uneven pie-shaped distribution in Fig. 11. As the propagation distance increases, the distribution range increases and the focused position rotates clockwise. Importantly, the rotation of the focused position becomes faster as the chirp factor increases.

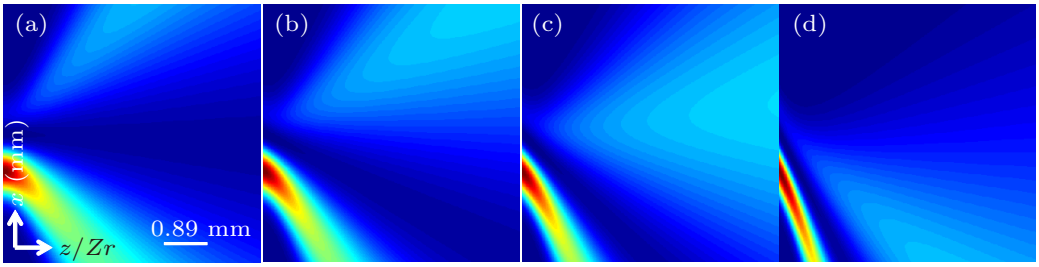


Fig. 9. All are the same as those in Fig. 2 except $\chi_0 = 1$.

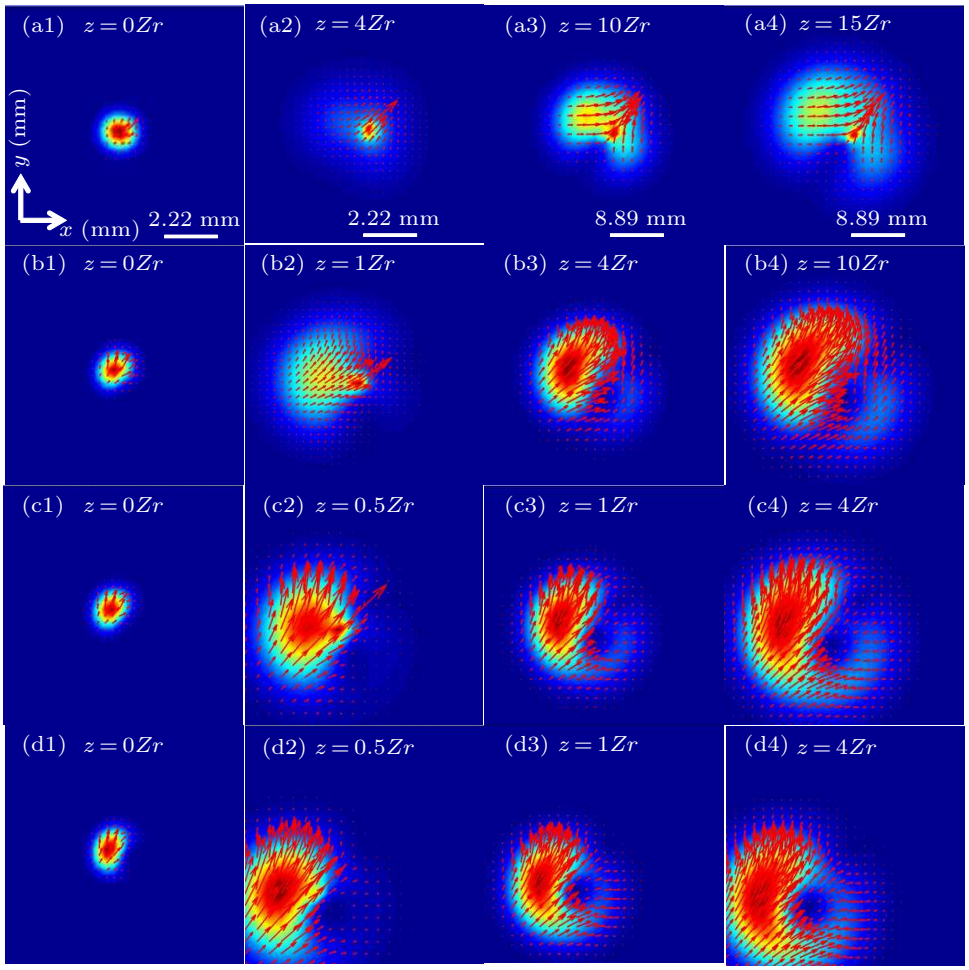


Fig. 10. All are the same as those in Fig. 4 except $\chi_0 = 1$.

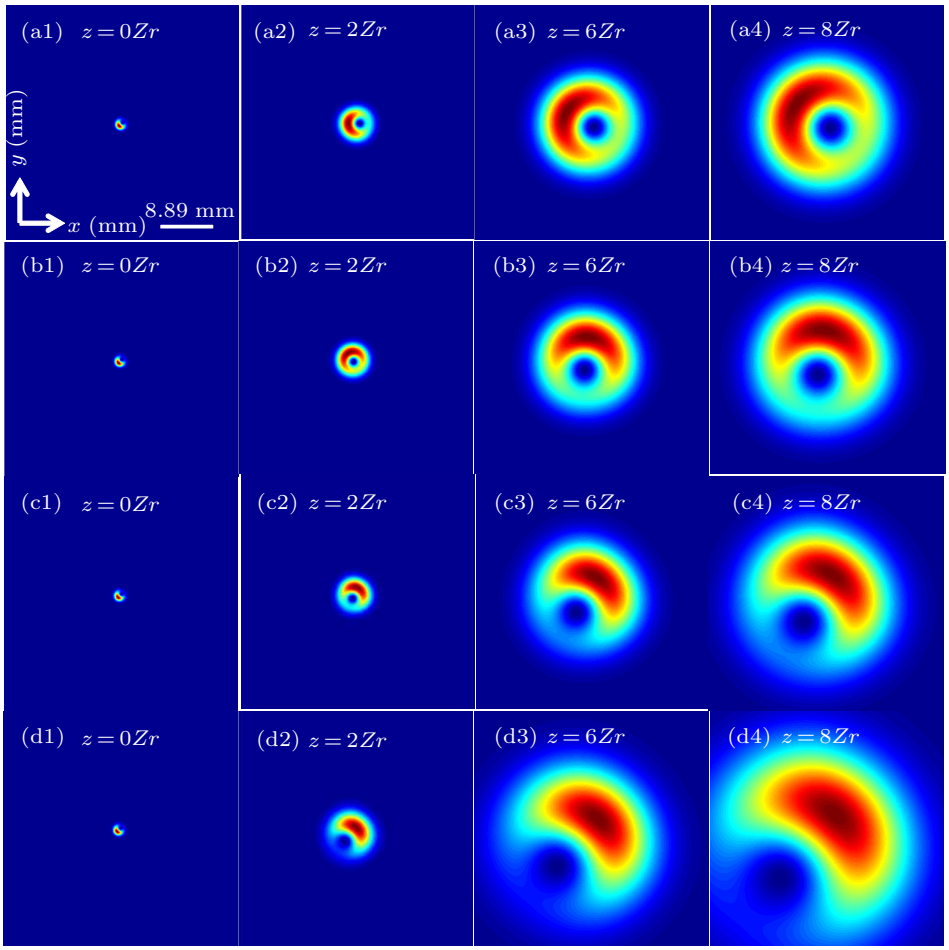


Fig. 11. All are the same as those in Fig. 5 except $\chi_0 = 1$.

4. Conclusion and perspectives

In this paper, we mainly discussed the influence of the chirp factor and the distribution factor to the CAiGVEP wave. When distribution factor is lower, the energy focuses on side lobes, converges from side lobes to main lobe, and then diffuses out from main lobe, forming a fan-shaped distribution in terms of the first-order CAiGVEP wave. But the difference is that the curvature of intensity distribution on the x–z plane becomes smaller as the chirp factor becomes larger, and the corresponding phase distribution is also quite different. The distribution of angular momentum density flow corresponds to the distribution of intensity. It is worth mentioning that the distribution of the second-order CAiGVEP wave reverses during propagation and reversal point in distance changes with the chirp factor. When distribution factor grows higher, the focus area rotates clockwise in a circular area and gets larger when the wave propagates. For angular momentum density flow, the direction of the main part tilts more towards the y axis as the chirp factor increases.

References

[1] Stix T H 1992 *Waves in plasmas* pp. 1–566
[2] Salandrino A and Christodoulides D N 2010 *Opt. Lett.* **35** 124913
[3] Gupta N and Singh A 2016 *Optik* **127** 8542
[4] Ouahid L, Dalil-Essakali L and Belafhal A 2018 *Optik* **154** 58
[5] Dolai B and Prajapati R P 2020 *Phys. Lett. A* 126462
[6] Berry M V and Balazs N L 1979 *Am. J. Phys.* **47** 264
[7] Siviloglou G A, Broky J, Dogariu A and Christodoulides D N 2008 *Opt. Lett.* **33** 90014
[8] Siviloglou G A and Christodoulides D N 2007 *Opt. Lett.* **32** 78349
[9] Wang L, Ji X, Deng Y, Li X, Wang T, Fan X and Yu H 2019 *Opt. Commun.* **441** 190
[10] Broky J, Siviloglou G A, Dogariu A and Christodoulides D N 2008 *Opt. Express* **16** 12880
[11] Baumgartl J, Mazilu M and Dholakia K 2008 *Nat. Photon.* **2** 675
[12] Panagiotopoulos P, Papazoglou D G, Couairon A and Tzortzakis S 2013 *Nat. Commun.* **4** 2622
[13] Hu D, Liang Y, Chen Y, Chen Z H and Huang X G 2017 *Opt. Commun.* **404** 196
[14] Xu C J, Hu H C, Liu Y J and Deng D M 2020 *Opt. Lett.* **45** 1451
[15] Bandres M A and Gutiérrez-Vega J C 2007 *Opt. Express* **15** 16719
[16] Melinger J S, Gandhi S R, Hariharan A, Tull J X and Warren W S 1992 *Phys. Rev. Lett.* **68** 2000
[17] Chremmos I and Giamalaki M 2015 *J. Opt. Sot. Am. A* **32** 867
[18] Shi X, Huang X, Deng Y, Tan C, Bai Y and Fu X 2017 *Opt. Commun.* **399** 16
[19] Xie J T, Zhang J B, Ye J R, Liu H, Liang Z Y, Long S J, Zhou K Z and Deng D M 2018 *Opt. Express* **26** 5845
[20] Zhou K Z, Zhang J B, Mo H R, Chen J H, Yang X L, Lai Z Y, Chen X Y, Yang X B and Deng D M 2018 *J. Opt.* **20** 075601
[21] Chen S J, Lin G, Xie J T, Zhen Y, Ma S and Deng D M 2019 *Opt. Commun.* **430** 364
[22] Yang X Y, Hong S H, Liang Z Y and Deng D M 2019 *Results in Physics* **15** 102691
[23] Mendonca J T 2012 *Phys. Plasmas* **19** 112113